Improvement of tensile and impact properties of 5083 aluminium weldments using fillers containing nano-Al_2O_3 and post-weld friction stir processing

M. Kianezhad[1] and A. Honarbakhsh Raouf[1]

Affiliation:
1 Faculty of Materials and Metallurgical Engineering, Semnan University, Semnan, Iran.

Correspondence to:
A. Honarbakhsh Raouf

Email:
ahonarbakhsh@semnan.ac.ir

Dates:
Received: 8 Mar. 2019
Revised: 17 Feb. 2020
Accepted: 28 Feb. 2020
Published: April 2020

How to cite:
Kianezhad, M., and Honarbakhsh Raouf, A.
Improvement of tensile and impact properties of 5083 aluminium weldments using fillers containing nano-Al_2O_3 and post-weld friction stir processing.
The Southern African Insitute of Mining and Metallurgy

DOI ID:
http://dx.doi.org/10.17159/2411-9717/662/2020

ORCiD ID:
M. Kianezhad:
https://orchid.org/0000-0003-2100-8733

A. Honarbakhsh Raouf:
https://orchid.org/0000-0002-0284-2573

Synopsis

A new technique was used to improve the properties of 5083 aluminium weldments using nano-Al_2O_3. The single-pass welded metals were made using gas tungsten arc welding by fillers containing different amounts of nano-Al_2O_3 particles fabricated using friction stir processing (FSP). To achieve a uniform distribution of nano-Al_2O_3 particles, FSP was applied to the welding zone. In comparison with parts welded with conventional filler wires, a 29% increase in yield strength, 18% increase in tensile strength, and a 56% increase in impact energy were attained in the specimens welded using filler wires containing nano-Al_2O_3 particles and post-weld FSP. The fracture mode of the weldments was changed from brittle (for the un-FSP'd specimens) to ductile (for the FSP'd specimens). Particles agglomeration, particle cracking, and weak matrix-reinforcement bonding reduce tensile properties. The impact fracture surface of the samples showed that the fracture mode of the FSP'd samples was ductile and the fracture was commonly initiated in the matrix. The uniform distribution of reinforcements leads to an improvement in the mechanical properties of the weldment.

Keywords
gas tungsten arc welding, filler metal fabrication, friction stir processing, 5083 aluminium alloy, impact energy, tensile fracture.

Introduction

The unique properties of 5083 aluminium, such as its light weight, high strength, and resistance to corrosion, make it an ideal material for use in marine industries and other structural applications. Thus, aluminium welding plays an important role in these industries. Due to melting and solidification as well as thermal effects on the surrounding area, the strength properties of the welding zone decrease. Different theories exist for strengthening mechanisms in metal matrix composites using nanoparticles. Adding nanoparticles to the welding zone leads to an increase in strength properties. However, the elongation and impact energy decrease (Mansoor and Shahid, 2015; Mazahery and Ostadshabani, 2011).

Fattahi *et al.*, (2012) studied the influence of Ti-containing inclusions on mechanical properties in multi-pass welding of a low-carbon steel. Results showed that by increasing the amount of titanium oxide nanoparticles in the electrode coating, the tensile properties and impact toughness of the welded parts improved. Fattahi *et al.*, (2013) developed a new technique for strengthening cold-worked aluminium in gas tungsten arc welding (GTAW). A filler metal containing multi-walled carbon nanotubes (MWCNT) produced by powder metallurgy was utilized to improve the mechanical properties of the welded metal. Fattahi *et al.*, (2015) used Al/TiC composite fillers fabricated by accumulative roll bonding (ARB) for the welding of aluminium and illustrated that the tensile strength of the welding zone was improved and the hardness increased from 64 to 93 Vickers micro hardness due to the use of Al/TiC composite fillers.

It should be pointed out that the existing processing techniques for the fabrication of nano-reinforced filler are based on liquid phase processing at high temperatures, powder metallurgy (PM), and severe plastic deformation. In liquid phase processing, it is hard to avoid the interfacial reaction between reinforcement and metal matrix and the formation of some detrimental phases. In the PM method, secondary processing methods such as extrusion and rolling are essential to fully consolidate the composite. The fabrication of nano-reinforced filler by most plastic deformation methods such as ARB is complicated. Friction stir processing (FSP) appears to offer another route to incorporate ceramic particles into the metal matrix to form bulk composites. The severe plastic deformation and material flow in the stirred zone (SZ) during FSP can be utilized to modify the bulk alloy composition through the mixing of other elements or second phases into the stirred alloys (Patel, Badheka, and

Kumar, 2016). FSP is characterized by unique features like the low amount of heat generated (processing temperature is below solidus temperature) and severe plastic deformation. Hence, FSP can be used to refine the microstructure of the welding zone (about 90% reduction in grain size of the welding zone) (Fuller and Mahoney, 2006), modify the casting structure, improve surface properties, increase the fatigue strength of the 5083 alumimium MIG fusion weld by 30% at 10^7 cycles (Fuller and Mahoney, 2006), and to achieve superplasticity in 5083 aluminium alloy (by 290% in elongation at 250°C) (Patel, Badheka, and Kumar, 2016).

Different studies have shown similar results regarding the improved mechanical properties of weldments achieved by adding nanoparticles in the welding zone (Fattahi *et al.*, 2013, 2014). However, the agglomeration of nanoparticles and the presence of welding defects (such as porosity) can lead to a decrease in mechanical properties, including strength, elongation, and fracture toughness. By employing FSP, the mechanical properties and microstructure can be improved (Mishra and Ma, 2005). FSP uses the method known as friction stir welding (FSW), which although it can be used to modify the local microstructure it does not join metal together (Ma, 2008). A number of studies have reported the effectiveness of FSP in casting and welding (Borrego *et al.*, 2014; Gregson and Harris, 2002). Fuller and Mahoney (2006) suggested that the application of FSP to aluminium weldments leads to an improvement in the tensile properties of 5083-H321/5356 arc welds. Kianezhad and Honarbakhsh Raouf (2019) showed that using a filler containing nano-Al_2O_3 particles and post-weld FSP led to an improvement in hardness and strength of the welding zone. In the present study, fillers containing different amounts of nano-Al_2O_3 particles were fabricated using FSP. The single-pass welds were made using GTAW. To achieve a uniform distribution of nano-Al_2O_3 particles, FSP was applied to the welding zone. Subsequently, tensile properties, impact energy, and the fracture surfaces of the weldments were evaluated.

Materials, methods, and tests

Materials and methods

Commercial aluminium alloy 5083 rolled plates with the chemical composition 5% Mg, 0.57% Mn, 0.15% Si, 0.35% Fe, 0.05% Cu, 0.05% Cr, and 0.02% Zn, (balance Al) were used as starting material. The 6 mm thick plates were cut to a size of 210 × 28 × 6 mm. Several grooves with a depth of 3.8 mm, 1 mm in width, and required length were machined on both sides of each strip and 30 nm nano-Al_2O_3 powder was inserted into each groove as shown in Figure 1a.

FSP was utilized for the production of welding fillers containing nano-Al_2O_3 particles as illustrated in Figure 1. To insert the nano-Al_2O_3 powders, five grooves with a depth of 3.8 mm, 1 mm in width, and the required length were machined on both sides of the plates. In order to prevent sputtering of Al_2O_3 powder and its ejection from the grooves during the process, the groove's gap was closed by a tool that had only a shoulder and no pin. To achieve a homogeneous distribution of nano-Al_2O_3 particles, samples were subjected to three passes of FSP for each path (shown in Figures 1b and 1c). All passes were carried out sequentially in the same direction. A hardened H-13 tool steel cylindrical threaded pin (5 mm in diameter; 4.5 mm in length,

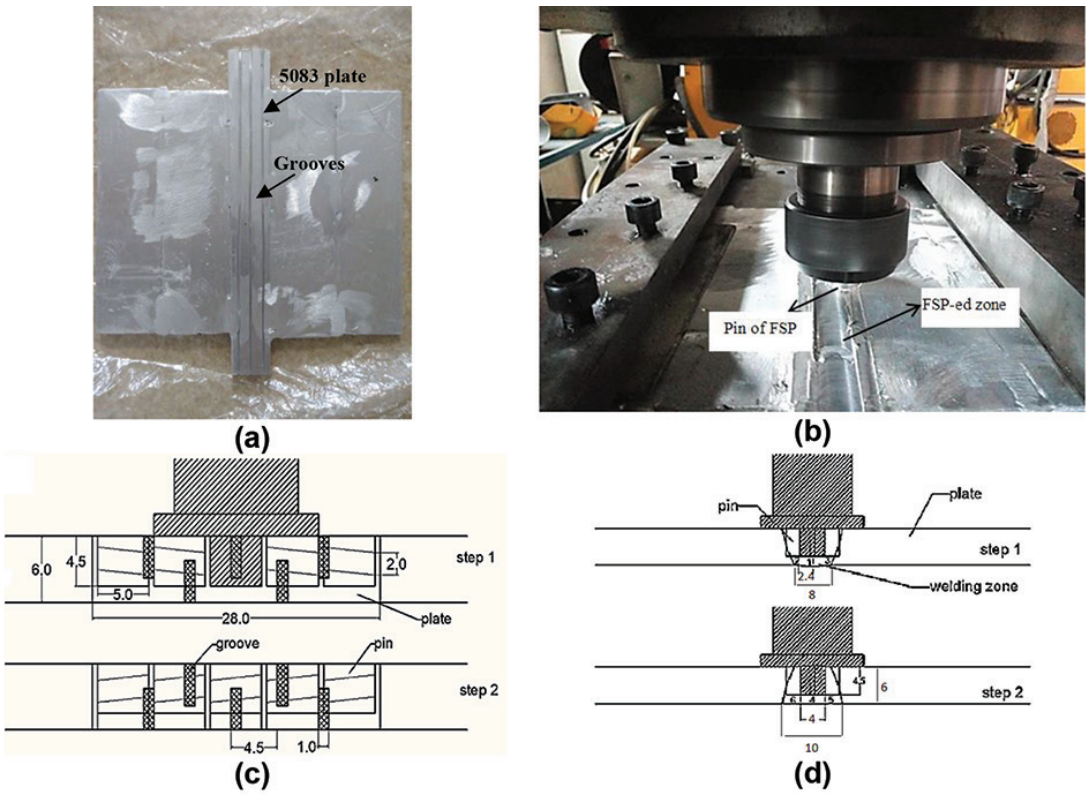

Figure 1—(a) Grooves utilized on 5083 aluminium to insert nanoparticles, (b) production of the composite filler using friction stir processing, (c) schematic of tool traverse along the strip, and (d) schematic view of the tool position relatively to the TIG welded plate

with a shoulder diameter of 16 mm) was used as the pin in FSP. FSP was performed with a rotation speed of 900 r/min, travel speed 28 mm/min, and a 5° tilting angle of the pin. Then, the plates were cut into 200 × 3 × 6 mm pieces, and fillers containing nano-Al_2O_3 particles were produced.

Sets of seven coupons of 5083-H112 aluminium alloy with a single V-shaped groove, width 6 mm, and an angle of 60° were welded using ER5183 filler metal (for conventional fusion welding) and fillers contained 0.75, 1.5, and 2.5% by volume nano-Al_2O_3 particles. The coupons were made using GTAW. Single-pass welding was carried out using a current of 140-160 A, voltage 20 V (AC), gas flow rate 13-15 l/min, and welding velocity of 1.6-1.9 mm/s. A groove angle of 60°, 6 mm deep, was used for welding under 100% Ar as the shielding gas. The surface of the welded zone was machined to eliminate the weld bead. To modify the local microstructure and obtain a homogeneous distribution of the reinforcing particles, FSP was performed on the welding zone using a cylindrical threaded hardened H-13 tool steel pin. The pin diameter, shoulder diameter, pin length, and tilt angle were 4 mm, 17 mm, 4.5 mm, and 5 degrees, respectively. The rotation speed of the pin was 1400 r/min, and the travel speed 28 mm/min. The tool traversed along the welding zone for three passes on each side. A schematic view of the process is shown in Figure 1d. All passes were carried out sequentially in the same direction, with no time for the sample to cool to room temperature. The following terminology was used to identify the test specimens: base (Al5083-H112 plate), simple weld (joint welded using ER5183 filler wire), and simple weld plus FSP (joint welded using ER5183 filler wire followed by six friction-stir passes). The specimens welded using fillers containing 0.75, 1.5, and 2.5 vol% nano-Al_2O_3 powders were identified by the numbers 0.75, 1.5, and 2.5, respectively, and the specimens identified as 0.75+FSP, 1.5+FSP and 2.5+FSP each underwent six friction-stir passes in the weld zone.

Test work

Three sub-sized tensile test specimens with 25 mm gauge length and 6 mm width were made from the weldment (the welding zone was in the middle of the tensile test specimen) according to ASTM B 557M. Tensile tests were performed using a SANTAM universal tensile test machine model STM-400, at a constant cross-head velocity and at room temperature of 20°C. The initial strain rate was 6.67×10^{-4} s^{-1}. The Charpy impact test was carried out at room temperature to evaluate the impact behaviour of the weldments. Sub-sized specimens ($10 \times 5 \times 55$ mm^3) with a 45° V-notch of 2 mm depth and 0.25 mm root radius at the FSP'd zone were made according to ASTM E23. Microstructural characterization was performed using optical microscopy (DM400 M model, Leica) and scanning electron microscopy (Mira3 model, TESCAN). For metallographic examination, the specimens were cross-sectioned perpendicular to the welding direction. After preparation, the specimens were etched with 50 ml of Poulton's reagent solution (12 ml HCl + 6 ml HNO_3 + 1 ml HF (40%) + 1ml H_2O) + 25 ml HNO_3 + 40 ml (3 g) CrO_3 in 100 ml H_2O) for 55 seconds in order to accentuate the grain boundaries. For observing different phases, the samples were etched with 0.5% HF solution for 7 seconds. For macroscopic observation, the samples were etched with 75 ml HCl + 25 ml HNO_3 + 5 ml HF + 25 ml distilled H_2O solution for 35 seconds (Kianezhad and Honarbakhsh Raouf, 2019). Dispersion of nano-Al_2O_3 particles was studied using a scanning electron microscope (SEM) equipped with silicon drift detector (SAMx) and energy dispersive spectroscopy (EDS). Also, fracture surface characterization of the samples was studied using the SEM.

Results and discussion

Tensile test properties

The yield strength, tensile strength, and elongation to fracture of different tensile test specimens are presented in Figure 2a. When the welding zone yield strength values are plotted as a function of the reciprocal square root of grain size of the welding zone, yield strength can be approximated through a Hall-Petch relationship as shown in Figure 2b.

The yield strength, tensile strength, and elongation of the weldments decreased from 175 MPa, 320 MPa, and 21% (for the base metal) to 131 MPa, 268 MPa, and 19% (for the 'simple weld' specimen), respectively, due to the equivalent cast arc-weld microstructure of the weldment (Fuller and Mahoney, 2006). Large grain size, the presence of welding defects, and residual stress can affect the mechanical properties of the welding zone. Adding nanoparticles to the welding zone (such as for the '1.5' specimen) slightly increased the yield strength of the welded part (about 8%), but the tensile strength and elongation were decreased (about 23% and 63%, respectively). In addition to the factors mentioned above, agglomerated nanoparticles are suitable sites for the nucleation of cracks and porosity (see Figure 3a).

Due to particle dispersion, large dislocation pile-ups occurred at the sites. The pile-ups will contribute to high stresses, the easy initiation of micro-cracks, and brittle behaviour (Dieter, 1988).

Application of FSP to the welding zone increased the yield strength, tensile strength, and elongation to fracture from 131 MPa, 268 MPa, and 19%, respectively, for the 'simple weld' specimen to 153 MPa, 304 MPa, and 23%, respectively, for the 'simple weld + FSP' specimen because of the grain refinement of the welding zone and the removal of welding defects (especially porosity) (Kianezhad and Honarbakhsh Raouf, 2019). The cross-sectional microstructure of the welding zones and FSP'd zones is illustrated in Figure 4. The grain size decreased from 94.7 µm (for the 'simple weld') to 4.9 µm (for the 'simple weld + FSP'). Fine and equiaxed grains were formed within the Al matrix because of the dynamic recrystallization during FSP (Huang *et al.*, 2016), which is caused by the frictional heat and intense plastic deformation of the material (see Figures 4a and 4b). Grain refinement by FSP could be a promising route to increase the yield strength (Karbalaei Akbari, Baharvandi, and Mirzaee, 2014; Patel, Badheka, and Kumar, 2016). The stress can be enhanced at grain boundaries due to the formation of dislocation pile-ups, and yielding takes place when the stress is large enough to cause the slip to propagate from one grain to the next (Hansen, 2004).

The presence of nano-Al_2O_3 particles and the post-weld FSP led to an improvement in the strength properties of the untreated weldments. The elongation to fracture decreased because of the presence of nano-Al_2O_3 particles in the welding zone. The maximum strength properties were attained in the '1.5 + FSP' specimen in comparison with the 'simple weld' specimen. Significant improvements in yield strength (29%) and tensile strength (about 18%) of the weldment were attained in the '1.5 + FSP' specimen, but the elongation to fracture decreased by 30%.

Also, in comparison with the 'simple weld + FSP' specimen, the yield strength and tensile strength were increased by 10.5% and 3.6%, respectively, but the elongation was decreased by

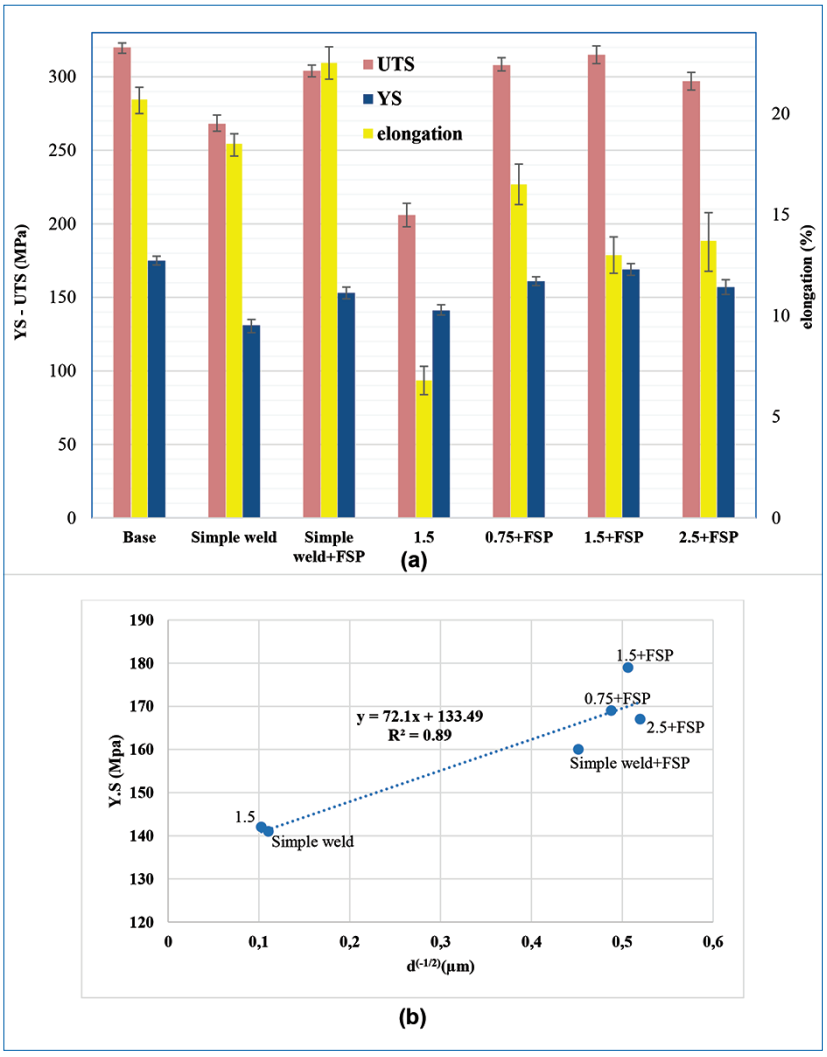

Figure 2—(a) The yield strength, tensile strength, and elongation to fracture of different tensile test specimens. (b) The yield strength of the welding zone plotted as a function of inverse, square-root of the grain size of the welding zone

42%. By applying FSP to the welding zone (welded by filler wires containing nanoparticles) the particles were uniformly dispersed in the matrix and the size of the reinforcements was decreased (see Figure 3b). During subsequent FSP passes, the plastic deformation of the material was more severe, and the stirred material deformed more easily, uniformly distributing the Al_2O_3 particles in the SZ. The uniform distribution of nanoparticles and fragmentation of clusters may be due to the more severe plastic deformation (Sharifitabar, 2011).

The small particle size and good distribution of the Al_2O_3 particles, which was confirmed by SEM micrographs, and low degree of porosity in the FSP'd specimens (see Figure 4) led to the effective transfer of applied tensile load to the uniformly distributed, strong Al_2O_3 particulates (Sharifitabar, 2011). Fine nano-Al_2O_3 particles are an important factor in the high strength of the weldment. Also, applying FSP to the welding zone decreased the size and aspect ratio of the other phases (see Figures 4c and 4d), and increased the quality of matrix-reinforcing particle bonding (Kianezhad and Honarbakhsh Raouf, 2019). Therefore, crack initiation at the sites was retarded.

The generation of dislocations due to the difference in the thermal expansion coefficients of the matrix and reinforcing particles and interaction of dislocations with nanoparticles (Orowan strengthening mechanism) increased the strain hardening rate and, therefore, improved the strength (Fattahi *et al.*, 2014). The removal of the welding defects, such as porosity (see Figures 4e, 4f, and 4g) and precipitation strengthening due to a higher volume of precipitates (*e.g.* Al-Fe-Mn) are also hypothesised to improve the mechanical properties of the weldment. For all the reasons stated, FSP led to an improvement in the mechanical properties (including strength and elongation) of the weldments.

Fractography of the tensile test specimens

Macroscopic fracture properties of the samples are listed in Table I. Macroscopic observation of the welded specimens containing nano-Al_2O_3 particles showed brittle fracture with flat surfaces; the breakdown position of the welded sample was at the middle of the tensile specimens and necking was not observed. The appearance of the fracture was granular and the strain to fracture was negligible. However, for the FSP'd specimens, a ductile fracture surface with shear angle of about 45° was observed. A small amount of necking occurred near the fracture surface, with a fibrous appearance.

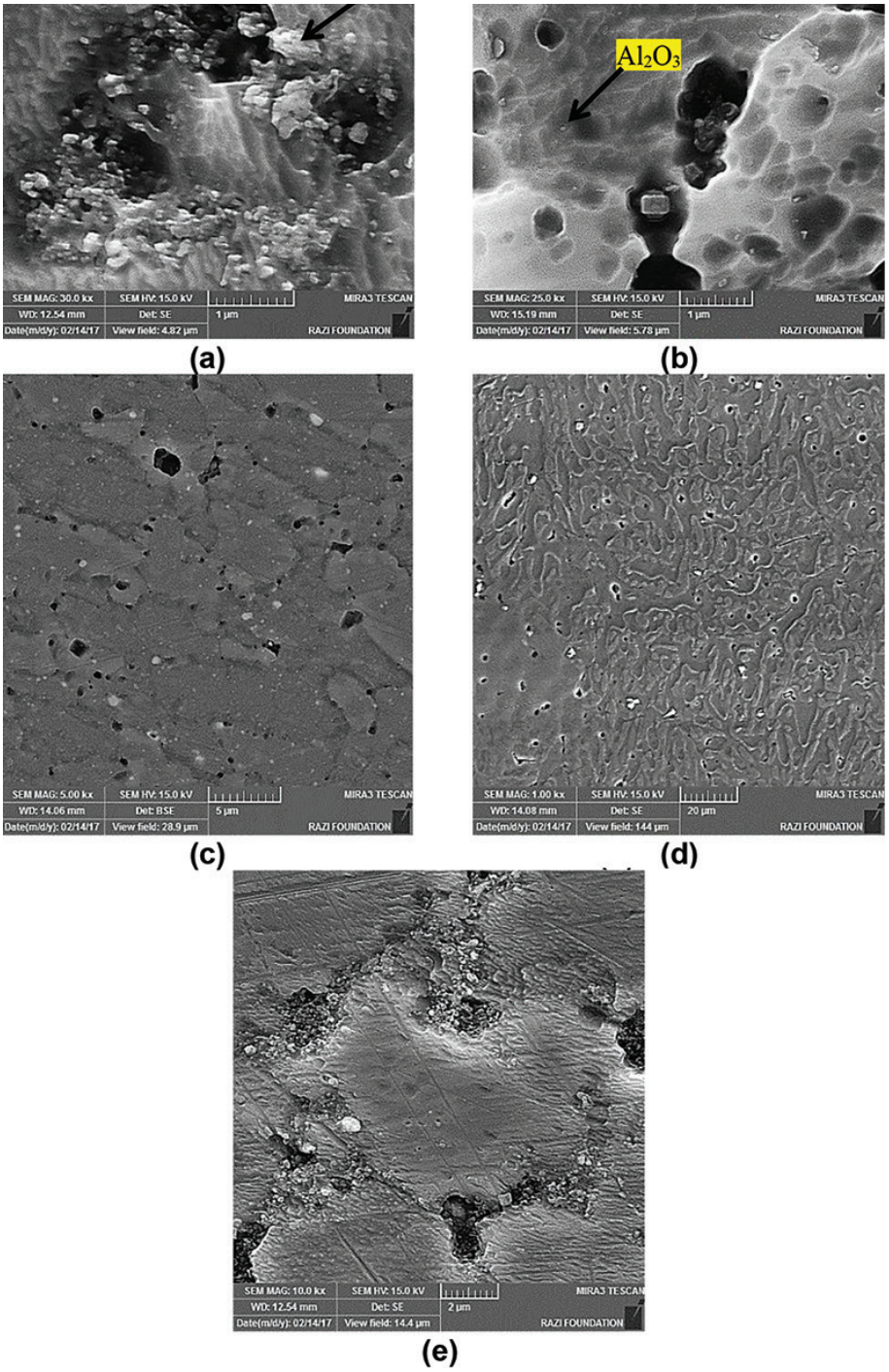

Figure 3—SEM micrographs of the welding zone containing nano-Al_2O_3 particles. (a) Agglomeration of nanoparticles in the welding zone of the '0.75' specimen, (b) and (c) the distribution of nanoparticles in '1.5 + FSP' specimen, (d) dendritic structure in the welding zone of the '1.5' specimen, and (e) the reinforcing particles were pushed by the solid/liquid to the front during solidification of the '1.5' specimen

SEM micrographs of tensile fracture surfaces of the un-FSP'd samples are shown in Figure 5. A large difference was seen in the appearance of the fracture surfaces of the samples. All the SEM micrographs were in good accordance with corresponding percentage elongation value in Figure 2a. For the 'base' sample (Figure 5a), dimples were fine with different sizes and depths. The relatively shallow dimples on the fracture surface of the alloy can be explained by both a much more uniform deformation in the alloy and the small size of inclusions in the materials. Larger dimples were formed in the 'simple weld' specimen (Figure 5b). Thus, voids were formed on some of the inclusions and were allowed to grow considerably and coalesce (Kang and Chan, 2004). By adding nano-Al_2O_3 particles to the welding zone, the fracture surface changed from dimple mode (for the 'simple weld' specimen) to semi-cleavage (for the '2.5' specimen) mode.

During deformation of these specimens, two types of micro-cracks will be initiated by the particles. Void nucleation can occur by de-cohesion of the matrix-reinforcement interface and cracked agglomerated reinforcing particles (Fuller and Mahoney, 2006). Once a reinforcement has cracked, any additional strain in that

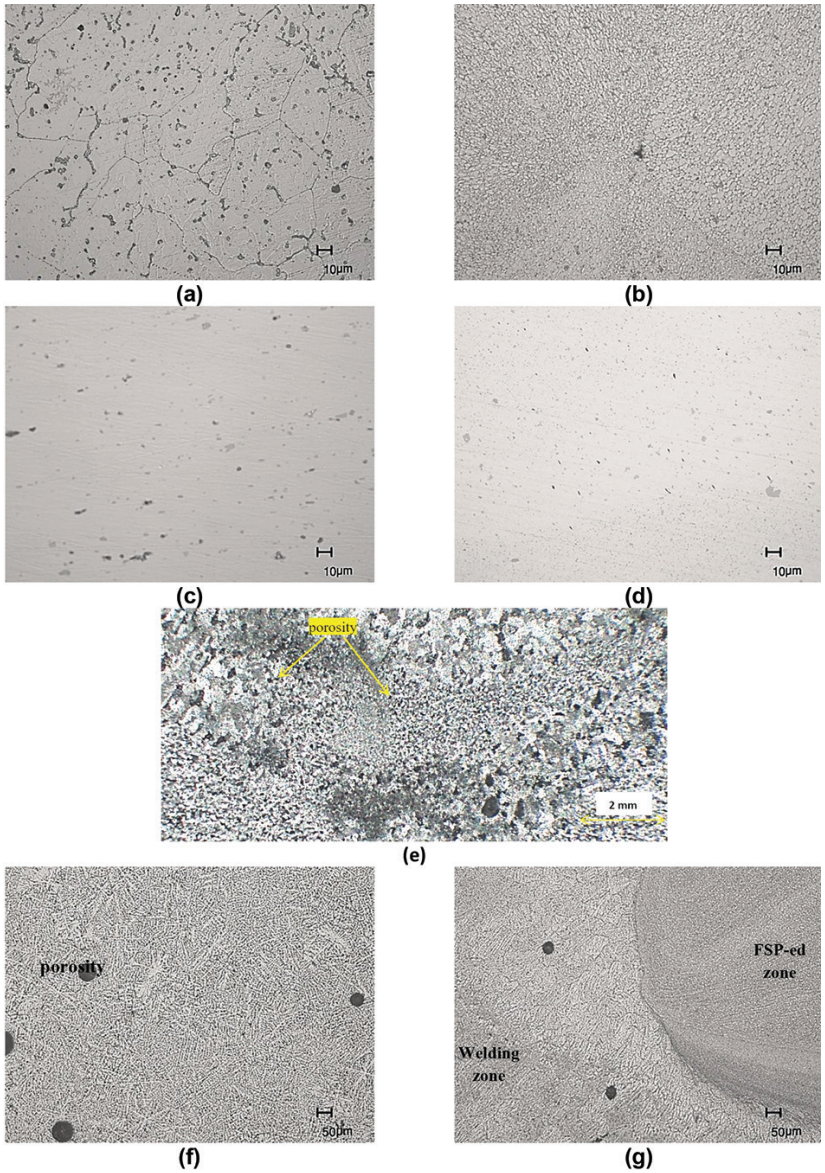

Figure 4—Optical micrographs of some of the samples. (a) Coarse grains in the '1.5' specimen, (b) refined grain of the nugget zone in the '1.5 + FSP' specimen, (c) difference in the size of various phases in the '1.5' specimen, (d) refined particles and inclusions of the nugget zone in the '1.5 + FSP' specimen, e.€ macro image of the weld cross-section in the '1.5' specimen, (f) The microstructure of the welding zone in the '1.5' specimen, and (g) the microstructure of the welding zone in the '1.5 + FSP' specimen

region can be accommodated by the opening of an interparticle void (Poza and Llorca, 1996). The fracture surfaces of the '1.5' specimen consisted of a bimodal distribution of flat facets and dimples as shown in Figure 5d. A mixture of dimples and flat surfaces implies reduced ductility in the '1.5' specimen. In most cases the large dimples (above 7 μm in mean diameter) contained second-phase particles. The presence of nano-Al_2O_3 particles at the bottom of some dimples (Figure 5e) showed that the agglomeration particulates provide sites for void nucleation (Kang and Chan, 2004).

A semi-cleavage fracture mode and micrograph of an Al_2O_3 cluster related to the '2.5' specimen are shown in Figure 5f. The change in the mode of fracture from dimple-ductile to quasi-cleavage can be related to the accumulation of nano-Al_2O_3 particles. The unfractured nano-Al_2O_3 particles were related to de-cohesion between the matrix and reinforcement. Al_2O_3 clusters do not bond strongly with the matrix. This leads to nucleation of micro-voids in the welding zone. Also, these clusters promote dislocation creation, stress concentration, and easy crack propagation at agglomerated particles, which have an effect on tensile properties. The presence of porosity (see Figure 4) in the welding zone can lead to matrix deterioration. During welding of the specimen with fillers containing nanoparticles, because the reinforcing particles were pushed by the solid/liquid to the front during solidification (see Figures 3c and 3d), the particles were segregated in the interdendritic region where the last step of solidification occurred (Zhong, 1996) and restricted the flow of liquid before the composite was completely solidified. Therefore, micro-cavities can be formed in these regions. Many cavities were produced by solidification, and deformation weakened the interdendritic regions (Zhong, 1996).

The tensile test fracture surfaces of the FSP'd specimens were dominated by dimples (see Figure 6). As seen in the 'simple weld' specimen, the homogeneity of the dimple sizes related to the

Table I

The macroscopic fracture properties related to the tensile test samples

Specimen	Appearance of fracture (fibrous/ granular)	Fracture angle (related to tensile axis)	Strain to fracture (brittle/ductile)	Fracture position	Yield stress of the weldment (MPa)
Base	Fibrous	45°	Ductile	-	175
Simple weld	Fibrous	About 45°	Ductile	Welding zone	131
Simple weld + FSP	Fibrous	45°	Ductile	Base metal (mostly)	153
0.75	Granular	Perpendicular	Brittle	Welding zone	-
1.5	Granular	Perpendicular	Brittle	Welding zone	141
2.5	Granular	Perpendicular	Brittle	Welding zone	-
0.75 + FSP	Dominantly fibrous	About 45°	Ductile	Welding zone (mostly)	161
1.5 + FSP	Dominantly fibrous	About 45°	Ductile	Welding zone (mostly)	169
2.5 + FSP	Dominantly fibrous	About 45°	Ductile	Welding zone	157

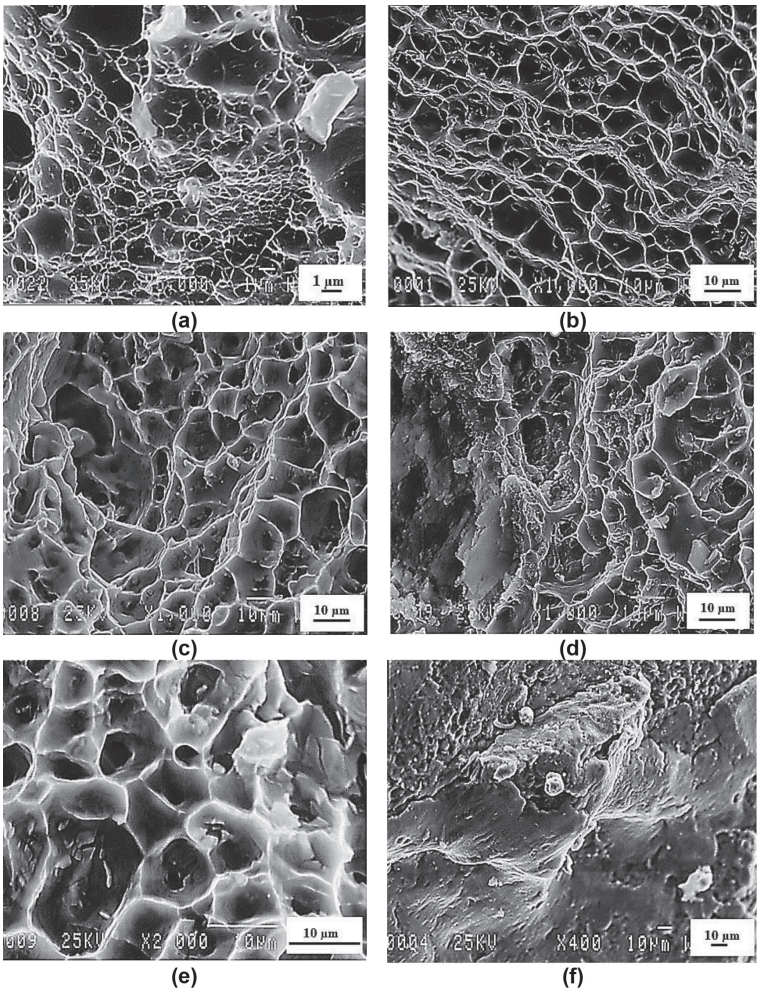

Figure 5 – SEM micrographs of fracture surfaces of the tensile test specimens. (a) 'Base', (b) 'simple weld', (c) '0.75', (d) '1.5', (e) inclusions and reinforcing particles at the bottom of the dimples in the '1.5' specimen, and (f) agglomerated nano-Al_2O_3 particles on the fracture surface of the '2.5' specimen

'simple weld + FSP' specimen decreased. The dimple size related to the 'simple weld + FSP' was very small due to the formation of ultrafine grains (Fattahi, 2014) and the fracturing of dispersed second phases. As mentioned before, SEM views of the area of the final fracture in the '1.5' specimen revealed dimples in some regions and cleavage plane facets in others. The dimples in the fracture surface of the '1.5 + FSP' specimen (Figure 6c) indicate that the ductility of the specimen was improved. The difference indicates more plastic deformation in the '1.5 + FSP' specimen than in the '1.5' specimen. However, for the '1.5 + FSP' specimen (see

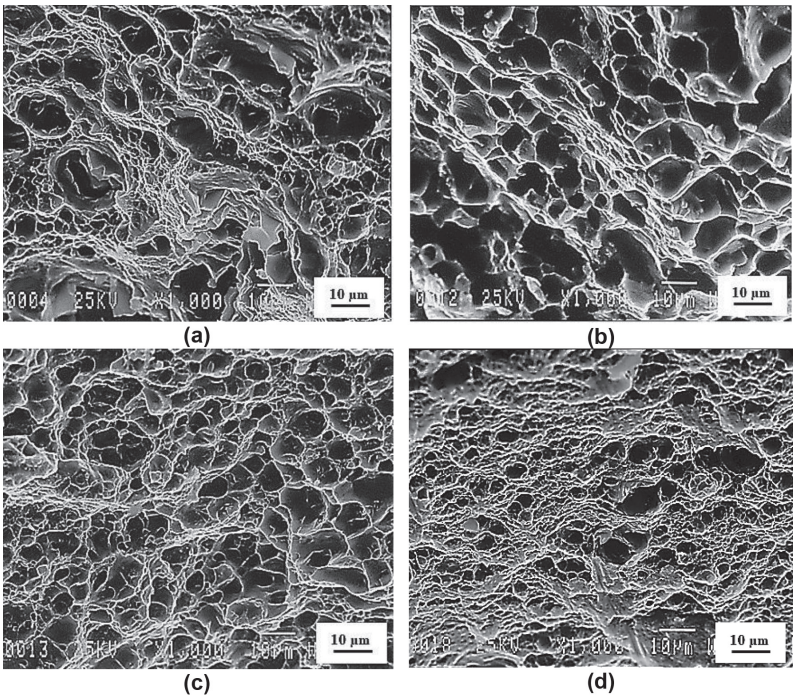

Figure 6—SEM micrographs of the fracture surfaces of the FSP'd specimens. (a) 'Simple weld + FSP',(b) '0.75 + FSP', (c) '1.5 + FSP', and (d) '2.5 + FSP'

Figure 6c), the centres of some dimples were free from any second-phase particles. Hence, micro-voids are basically initiated in the matrix instead of particles or particle-matrix interface. Final failure occurred by coalescence of small voids in the matrix.

There is a similar situation for other FSP'd specimen as shown in Figure 6. For the '2.5' specimen, the fracture mode was basically cleavage. Shallow dimples were observed in some areas of the welding zone. Ductile fracture morphology was found in the '2.5 + FSP' sample, which confirms the improvement in ductility. Among the FSP'd specimens containing nano-Al_2O_3 particles, there were some notably differences between the size and depth of dimples. The fracture surface of the '2.5 + FSP' specimen consisted of finer dimples than other FSP'd specimens, which correlated with the amount of nano-Al_2O_3 particles in the welding zone.

Impact test properties

Macroscopic photographs of fracture surfaces of the impact test specimens are shown in Figure 7. The lateral expansion shows that the fracture is ductile. Figure 8 shows SEM micrographs of impact test fracture surfaces of some specimens. All the fracture surfaces presented a ductile fracture morphology involving the nucleation, growth, and coalescence of voids. There are voids and dimples in different sizes and shapes in the fracture surfaces.

Figure 8 shows that by increasing the nanoparticle content in post-weld FSP specimens, the size of the dimples decreased. The presence of second-phase particles at the bottom of some dimples indicates that fracture was basically initiated in the particles. The particles are suitable for micro-crack nucleation.

The weldment impact energy of the specimens is shown in Figure 9. Also, the strength *versus* impact energy of the samples is shown in Figure 10. It can be seen that the impact energy is increased by increasing the strength properties of the samples. The results show that the impact energy of aluminium

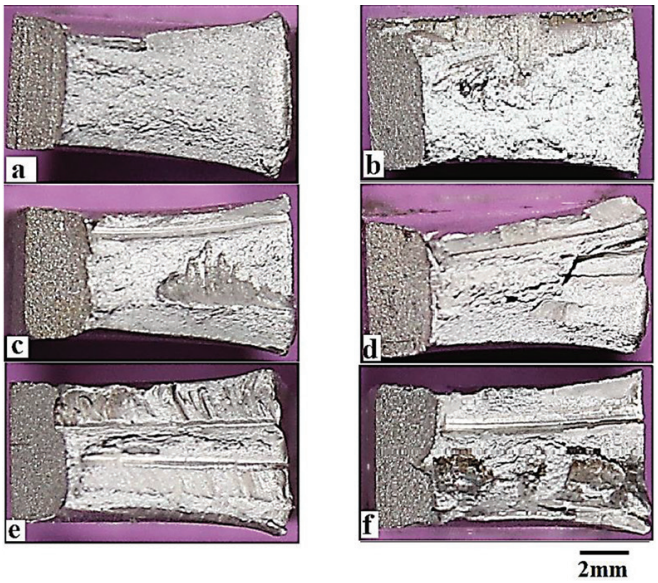

Figure 7—Macroscopic photographs of fracture surfaces of the impact test specimens. (a) 'Base', (b) 'simple weld', (c) 'simple weld + FSP', (d) '0.75 + FSP', e '1.5 + FSP', and (f) '2.5 + FSP'. The lateral expansion and fibrous appearance indicate that the fracture mode is ductile

weldments with 5183 filler metals was significantly reduced due to coarsening in the grain structure of the matrix material and the presence of welding defects. The appearance of pores in the matrix degraded the impact energy of the welding zone, because pores can act as micro-crack initiators during deformation. Maximum impact energy among the FSP'd specimens was found in the 'simple weld + FSP' specimen. The application of FSP to the welding zone increased the impact energy by 68%. Compared to the 'simple weld', the impact energy of the '0.75 + FSP', '1.5 + FSP', and '2.5 + FSP' specimens increased by 56%, 34%,

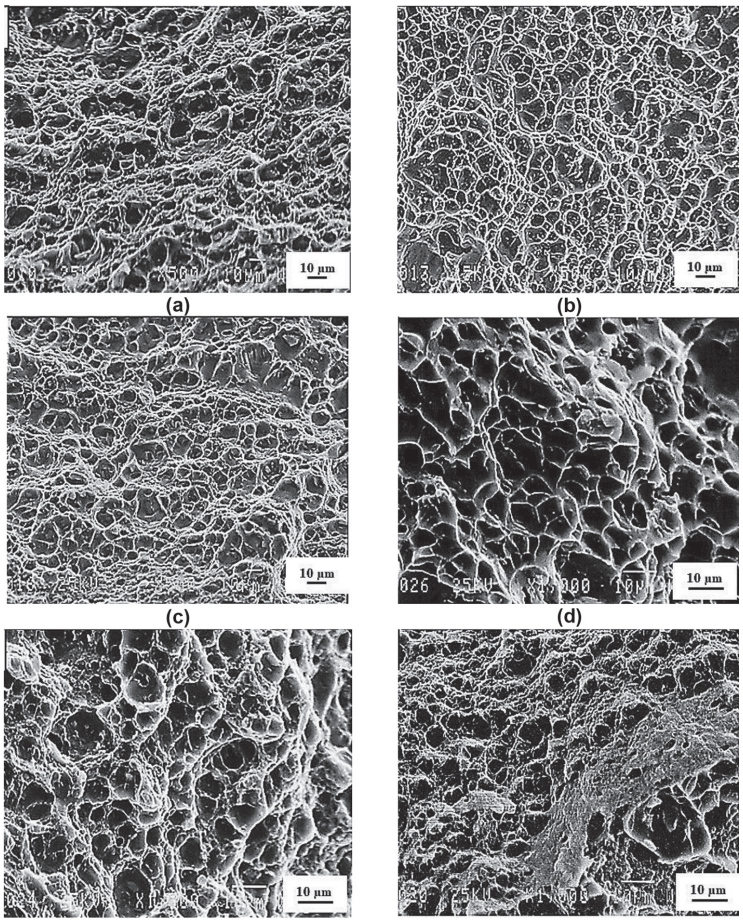

Figure 8—SEM micrographs of impact test fracture surfaces. (a) Base', (b) 'simple weld', (c) 'simple weld + FSP', (d) '0.75 + FSP', e '1.5 + FSP', and (f) '2.5 + FSP'

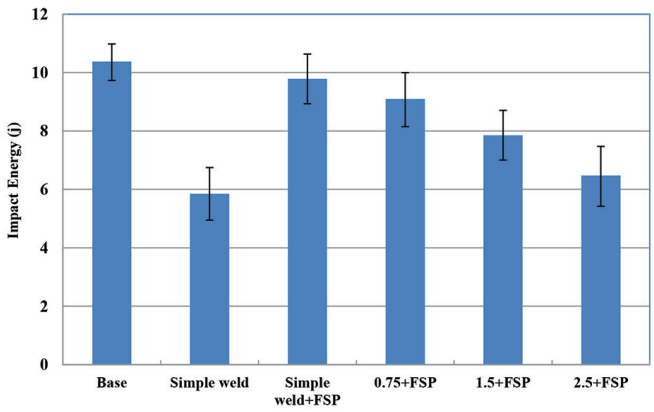

Figure 9—The impact energy of the specimens (at least three samples per condition)

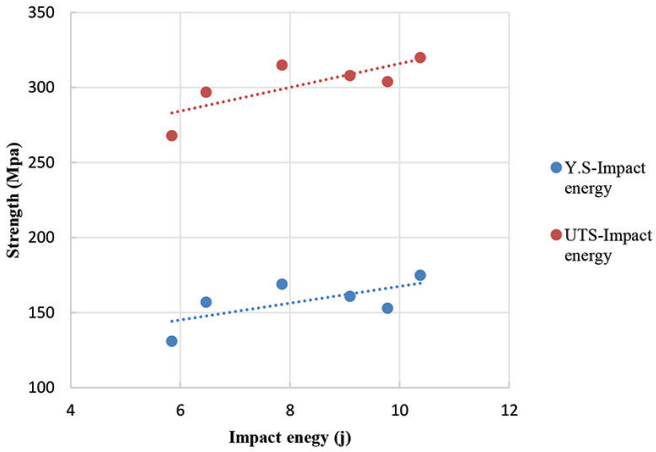

Figure 10—The strength of the samples *versus* impact energy

and 10%, respectively. This was due to grain size refinement, removal of the welding defect, homogeneous distribution of and decrease in the size and the aspect ratio of the second phases (which increased resistance to cracking (Dieter, 1988) during FSP. Increasing the amount of nano-Al_2O_3 particles decreased the impact energy of the weldment. The lower impact energy of these specimens can be attributed to the presence of brittle reinforcing particles, which may act as a stress concentration area (Ozden, 2007).

Conclusions

- Adding nano-Al_2O_3 particles to the welding zone led to a deterioration in the tensile properties of the weldment. The fracture surface was changed from ductile mode (for the 'simple weld' specimen) to semi-cleavage mode (for the '2.5' specimen containing nanoparticles), which could be related to the accumulation of nano-Al_2O_3 particles. The unfractured nano-Al_2O_3 particles were related to de-cohesion between the matrix and reinforcement.

- Applying FSP to weldments significantly improved performance in terms of yield and ultimate strengths, as well as elongation (by 21%). The yield strength improvement of some 17% could prove useful in higher stressed weld areas. Also, the presence of nano-Al_2O_3 particles and the post-weld FSP led to an improvement in the yield strength and ultimate strength properties of the weldments (by 29% and 17.5% respectively). The elongation to fracture decreased because of the presence of nano-Al_2O_3 particles in the welding zone.
- In comparison to the weldment welded with ER5183 filler wires, a 29% increase in yield strength, 18% increase in tensile strength, and a 30% decrease in elongation were attained in the specimens welded using filler wires containing nano-Al_2O_3 particles and post-weld FSP. The tensile test fractured surfaces of the FSP'd specimens were dominated by dimples. Micro-voids were basically initiated in the matrix instead of at particles or the particle-matrix interface. Final failure occurred by coalescence of small voids in the matrix. Increasing the concentration of nano-Al_2O_3 particles in the FSP' specimen led to finer dimples.
- Applying FSP to the welding zone led to an improvement in the impact energy of the weldment by up to 68%. Moreover, in comparison with the 'simple weld', the impact energies of the '0.75 + FSP', '1.5 + FSP', and '2.5 + FSP' specimens increased by 56%, 34%, and 10%, respectively. The lower impact energies of these specimens can be attributed to the presence of brittle reinforcing particles, which may act as a stress concentration area. The impact test fracture surfaces of FSP'd specimens were dominated by dimples. By increasing the nanoparticle concentration in the welding zone, the size of the dimples decreased. The presence of second-phase particles at the bottom of some dimples showed that the cracks were basically initiated in the particles.
- Grain size refinement of the welding zone, removal of the welding defect, the generation of dislocations, increasing the quality of matrix-reinforcing particle bonding, and homogeneous distribution and decreased aspect ratio of the second-phase particles during FSP contributed to an improvement in the mechanical properties, including strength, elongation, and fracture toughness of the weldments.

Acknowledgments

The authors would like to thank Semnan University and Iran Nanotechnology Initiative Council for financial support.

References

Borrego, L.P., Costa, J.D., Jesus, J.S., Loureiro, A.R., and Ferreira, J.M. 2014. Fatigue life improvement by Friction Stir Processing of 5083 aluminium alloy MIG butt welds. *Theoretical and Applied Fracture Mechanics*, vol. 70. pp. 68–74.

Dieter, G.E. 1988. Mechanical Metallurgy (SI Metric Edition). McGrew-Hill, UK.

Fattahi, M., Gholami, A.R., Eynalvandpour, A., Ahmadi, E., Fattahi, Y., and Akhavan S. 2014. Improved microstructure and mechanical properties in gas tungsten arc welded aluminum joints by using graphene nanosheets/aluminum composite filler wires. *Micron*, vol. 64. pp. 20–27.

Fattahi, M., Mohammady, M., Sajjadi, N., Honarmand, M., Fattahi Y., and Akhavan, S. 2015. Effect of TiC nanoparticles on the microstructure and mechanical properties of gas tungsten arc welded aluminum joints, *Journal of Materials Processing Technology*, vol. 217. pp. 21–29.

Fattahi, M., Nabhani, N., Hosseini, M., Arabian, N., and Rahimi, E. 2012. Effect of Ti-containing inclusions on the nucleation of acicular ferrite and mechanical properties of multipass weld metals. *Micron*, vol. 45. pp. 107–114.

Fattahi, M., Nabhani, N., Rashidkhani, E., Fattahi, Y., Akhavan S., and Arabian, N. 2013. A new technique for the strengthening of aluminum tungsten inert gas weld metals: Using carbon nanotube/aluminum composite as a filler metal. *Micron*, vol. 54-55. pp. 28–35.

Fuller C.B. and Mahoney, W.M. 2006. The effect of friction stir processing on 5083-H321/5356 Al arc welds: Microstructural and mechanical analysis. *Metallurgical and Materials Transaction A*, vol. 37. pp. 3605–3615.

Gregson P.J. and Harris, S. 2002. The stability of the nugget zone grain structure in AA7010 alloy friction stir welds during solution treatment. *Materials Science Forum*, vol. 396-402. pp. 1549–1554.

Hansen, N. 2004. Hall–Petch relation and boundary strengthening, *Scripta Materialia*, vol. 51. pp. 801–806.

Huang, C., Li, W., Zhang, Z., Fu, M., Planche, M., Liao H., and Montavon, G. 2016. Modification of a cold sprayed SiCp/Al5056 composite coating by friction stir processing. *Surface & Coatings Technology*, vol. 296. pp. 69–75.

Kang Y.C.and Chan, S.L. 2004. Tensile properties of nanometric Al_2O_3 particulate-reinforced aluminum matrix composites. *Materials Chemistry and Physics*, vol. 85. pp. 438–443.

Karbalaei Akbari, M., Baharvandi, H.R., and Mirzaee, O. 2014. Investigation of particle size and reinforcement content on mechanical properties and fracture behavior of A356-Al_2O_3 composite fabricated by vortex method. *Journal of Composite Materials*, vol. 48, no. 27. pp. 3315–3330.

Kianezhad M. and Honarbakhsh Raouf, A. 2019. Effect of nano-Al_2O_3 particles and friction stir processing on 5083 TIG welding properties, *Journal of Materials Processing Technology*, vol. 263, pp. 356–365.

Ma, Z.Y. 2008. Friction stir processing technology: A review. *Metallurgical and Materials Transactions A*, vol. 39. pp. 642–658.

Mansoor, M. and Shahid, M. 2015. Fractographic evaluation of crack initiation and growth in Al-CNTs nanocomposite fabricated by induction melting. *Acta Physica Polonica A*, vol. 128. pp. 276–279.

Mazahery, A. and Ostadshabani, M. 2011. Investigation on mechanical properties of nano-Al_2O_3-reinforced aluminum matrix composites. *Journal of Composite Materials*, vol. 45. pp. 2579–2586.

Mishra, R.S. and Ma, Z.Y. 2005. Friction stir welding and processing, *Materials Science and Engineering A*, vol. 20. pp. 1–78.

Ozden, S., Ekici R., and Nair, F. 2007. Investigation of impact behaviour of aluminum based SiC particle reinforced metal-matrix composites. *Composites Part A*, vol. 38. pp. 484–494.

Patel, V., Badheka, V., and Kumar, A. 2016. Friction stir processing as a novel technique to achieve superplasticity in aluminum alloys: Process variables, variants, and applications. *Metallography and Microstructural Analysis*, vol. 5. pp. 278–293.

Poza, P. and Llorca, J. 1996. Fracture toughness and fracture mechanisms of Al-Al_2O_3 composites at cryogenic and elevated temperatures. *Materials Science and Engineering Ai*, vol. 206. pp. 183–193.

Sharifitabar, M., Sarani, A., Khorshahian, S., and Shafiee Afarani, M. 2011. Fabrication of 5052Al/Al_2O_3 nanoceramic particle reinforced composite via friction stir processing route. *Materials and Design*, vol. 32. pp. 4164–4172.

Zhong, W.M., L'Esperance, G., and Suery, M. 1996. Effect of thermornechanical processing on the microstructure and mechanical properties of Al-Mg (5083)/SiCp and Al-Mg (5083)/$A1_2O_3$p composites. Part 3: Fracture mechanisms of the composites. *Materials Science and Engineering A*, vol. 214. pp. 104–114. ◆